Appl Phys A (2013) 111:1065–1070
DOI 10.1007/s00339-012-7493-2

Applied Physics A
Materials Science & Processing

Top electrode material related bipolar memory and unipolar threshold resistance switching in amorphous Ta_2O_5 films

Yunyu Cai · Cuicui Sheng · Changhao Liang

Received: 12 September 2012 / Accepted: 3 December 2012 / Published online: 16 December 2012

Abstract Tantalum oxide (Ta_2O_5) is one of the most studied materials for its stable resistance switching and potential application in nonvolatile memory devices. Top electrode and essential switching material are two critical points dominating its switching characteristics. Here, Ta_2O_5 films of amorphous nature (a-Ta_2O_5) with tunable thicknesses were made by changing the applied voltage during anodic oxidation of Ta-metal foils. The resistance-switching behavior of an a-Ta_2O_5 film in a metal/a-Ta_2O_5/Ta configuration was investigated by using a sputtered W or Ag metal film as the top electrode. The unipolar threshold switching phenomenon was observed using W as top electrode (W_{TE}), while bipolar switching behaviors were achieved using active Ag metal as top electrode (Ag_{TE}). The thickness of the a-Ta_2O_5 film shows an obvious effect on the SET voltage in a W_{TE}/a-Ta_2O_5/Ta device. The interfacial redox reaction induced formation of more conductive Ta-rich suboxide and the Joule heating effect are proposed to contribute to the unipolar threshold switching behavior. It is also suggested that the bipolar switching could have resulted from the electrochemical reaction-induced dissolution and growth of Ag conducting channels inside the Ta_2O_5 films.

1 Introduction

Reversible resistance switching in a metal/insulator/metal structure has attracted an increasing amount of scientific attention because of its rich physics and potential application in nonvolatile memories [1, 2]. Conductivity switching behaviors controlled by external voltages have been investigated in many binary and ternary metal oxide films, such as NiO [3], TiO_2 [4], CoO [5], GeO_x [6], ZnO [7], and $SrTiO_3$ [8] due to the promising scalability, retention, and plenty of switching characteristics of these materials. Most of these oxides were prepared using techniques such as sputter deposition, sol–gel method, or pulsed laser deposition. Anodic oxidation is an easy and cost-effective technique for growing reliable and controllable oxide films. However, only a few studies have been focused on the resistance switching in anodic oxidized amorphous thin films [9].

It is also recognized that the reactivity and top electrode-related interfacial reaction should have important effects on the switching characteristics. The unipolar and bipolar resistance-switching (RS) behaviors of Me/TiO_2/Pt structures have been observed by altering the material of the top electrode (TE) [10]. The unipolar and bipolar switching behaviors with similar materials, such as TiO_2 [11], NiO [12], and ZrO_2 [13–15], have also been investigated. In addition, the key role of oxygen nonstoichiometry and oxygen-deficient oxide phases as the underlying mechanism of the resistance change has been discussed for many oxides. Ta_2O_5 is a high-k dielectric material that has been extensively studied for its reliable and potential resistance-based memory applications [16–19]. However, less effort has been made in the investigation of resistance-switching mode polarity in anodic amorphous Ta_2O_5 films with plenty of oxygen vacancies.

In this paper, we report the facile fabrication of thickness-tunable Ta_2O_5 thin films. Then, the unipolar threshold switching and bipolar memory switching behaviors of metal/a-Ta_2O_5/Ta sandwich structures are investigated by using W and Ag metals as top electrodes, respectively. Fi-

Y. Cai · C. Sheng · C. Liang (✉)
Key Laboratory of Materials Physics and Anhui Key Laboratory of Nanomaterials and Nanotechnology, Institute of Solid State Physics, Hefei Institutes of Physical Science, Chinese Academy of Sciences, Hefei 230031, China
e-mail: chliang@issp.ac.cn
Fax: +86-551-65591434

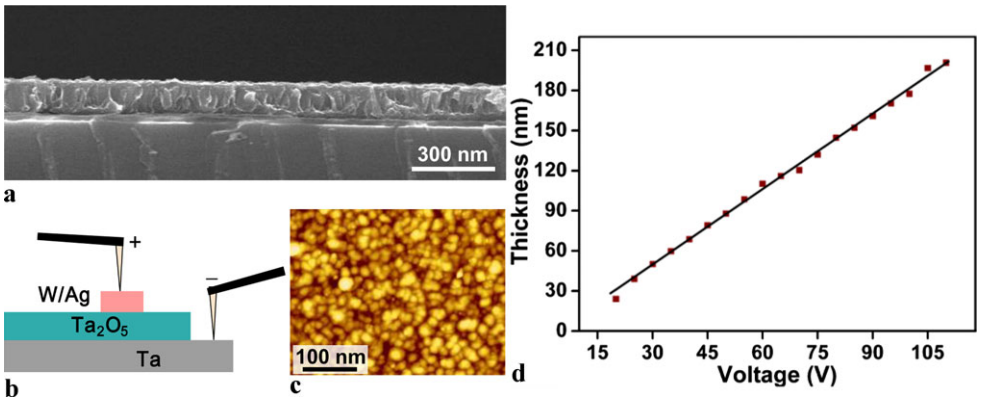

Fig. 1 (**a**) Typical SEM image of the surface of an anodic Ta_2O_5 film. (**b**) Schematic view of a nanometer-scale switch consisting of a Ta_2O_5 thin film sandwiched between the W/Ag *top* electrode and the *bottom* Ta electrode. (**c**) AFM topography image of Ta_2O_5 film surface. (**d**) Linear relationship between film thickness and anodic voltage

nally, the switching mechanisms will be discussed by considering the evolution of interfacial reaction-induced localized anion-deficient channels and metallic conducting filaments (CFs).

2 Experimental details

Prior to anodic oxidation, 0.25-mm-thick high-purity Ta sheets (99.99 %) were sequentially degreased via sonication in acetone and alcohol solutions, respectively. The Ta sheets were then rinsed with distilled water and dried in air. The samples were electrochemically polished at 15 V in a mixture of concentrated H_2SO_4 and 48 % aqueous HF solution at a 9:1 volumetric ratio for 20 min to smooth the surface [20]. Anodic oxidation of Ta was conducted in a 1 M H_2SO_4 solution at room temperature for 20 min using different voltages with a graphite plate as the counter electrode [21]. After anodic treatment, the samples were washed with distilled water and dried in an air stream. The thicknesses of the Ta films oxidized at different voltages were determined based on a UVISEL ER spectroscopic ellipsometer. The surface topographical image of the films was examined by an atomic force microscope (AFM, Seiko SPI3800N).

Compositional analyses were performed using grazing incidence X-ray diffractometry (GIXRD) with an X'Pert instrument (Cu K_α, $\lambda = 1.54059$ Å). Surface valence states of the anodic oxide films were analyzed by X-ray photoelectron microscopy (XPS), using an Al K_α source. All binding energy values were calibrated using contamination carbon (284.6 eV) as reference.

The resistance-switching behaviors of the anodic oxidized Ta_2O_5 films were investigated using an Agilent B1500A semiconductor parameter analyzer by connecting the bottom and top electrodes of the samples through a probe system. The top Ag and W circular electrodes with the same geometry and thickness of approx. 30 nm were made by sputtering through a circle-shaped mask (25 μm in diameter).

3 Results and discussion

Figure 1a shows the typical Field Emission Scanning Electron Microscope (FE-SEM) cross-sectional image of a Ta sheet after anodic oxidation in a dilute H_2SO_4 solution. A compact and uniform oxide layer that consisted of nanoscale particles (inset SEM image) was observed after anodic oxidation, which is further configured with the top electrode to form a sandwich-like system for electrical properties' measurements (Fig. 1b). Figure 1c shows the atomic force microscopy (AFM) topographic image of the a-Ta_2O_5 film surface. The film clearly consisted of nanoparticles with uniform size. Figure 1d shows the measured voltage range and the relationship between the film thickness and the applied voltage, which was determined via spectroscopic ellipsometer measurements. The thicknesses of the compact Ta_2O_5 films in the range of 30–200 nm were linearly dependent on the anodizing voltage.

X-ray diffraction (XRD) and XPS measurements were used to investigate the phase structure of passive oxide films. In the XRD pattern, aside from metallic Ta diffraction peaks, no other diffraction peaks were observed (not shown here). It indicated that the anodic film formed is predominantly of an amorphous nature. The XPS spectra of TaO_x films is shown in Fig. 2; the binding energies of the two Ta peaks are located at 26.04 and 27.84 eV, indicating that Ta in oxide films is mainly in a valence state of Ta^{5+}. The calculated atomic ratio of O/Ta from the TaO_x spectra is obviously less than the theoretical value of Ta_2O_5. Deficient oxygen might result from the existence of trace amounts of suboxidation states of Ta, such as Ta^{4+}. The XPS and XRD analyses demonstrated that an amorphous Ta_2O_5 compact film was obtained using a simple anodic oxidation technique.

A schematic diagram of the sandwich structure is shown in the inset of Fig. 1b. The current–voltage (I–V) characteristic curves (Fig. 3a to c) were measured using a tungsten-alloy probe in direct contact with the top electrode of a $W_{TE}/Ta_2O_5/Ta$ system (TE, top electrode). The driving voltage on the top electrode was biased, while the bottom

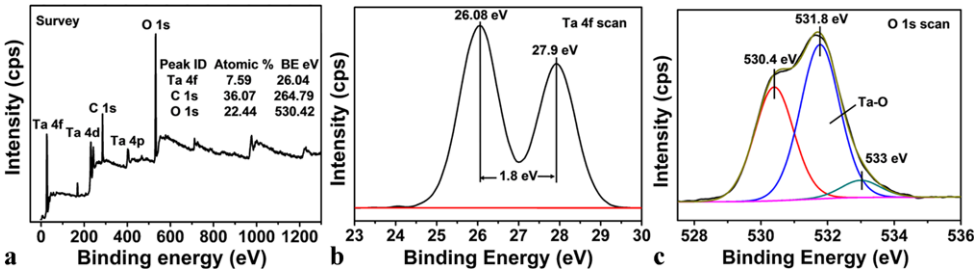

Fig. 2 XPS spectra of TaO_x films obtained by anodic oxidation: (**a**) all-survey XPS spectrum of TaO_x films. (**b**) High-resolution XPS $4f_{7/2}$ and $4f_{5/2}$ spectra, with binding energies located at 26.04 and 27.84 eV. (**c**) Valence band spectra of O after Gaussian fitting

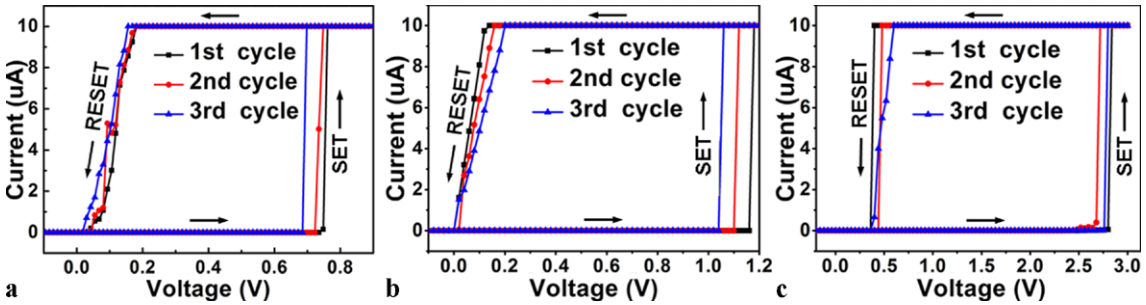

Fig. 3 Hysteretic current–voltage (*I–V*) *curves* of the W_{TE}/a-Ta_2O_5/Ta structures with different Ta_2O_5 layer thicknesses at room temperature. The *arrows* indicate the voltage sweeping direction

electrode was grounded. The compliance current was limited to 10 μA during voltage sweeps to prevent the breakdown and destruction of the structures. *I–V* curves from TaO_x films with different thickness were investigated for several consecutive voltage sweeps. The asymmetric *I–V* curves show a typical unipolar resistance-switching characteristic. It is seen that the output current began to increase abruptly from several pA to the compliance current of 10 μA at a SET voltage (V_{set}) when the voltage was swept from $-V_{max} \rightarrow 0 \rightarrow V_{max}$. However, the current abruptly decreased to tens of nA at a RESET voltage (V_{reset}) when the voltage was swept in the opposite direction. The low-resistance state (LRS) was initially set by applying a positive voltage. Almost all of the reset voltages of the devices existed in the positive-bias region; there is no obvious device state change by sweeping the voltage in the negative-bias region, as shown in Fig. 3a to c. No reversible resistance switching was observed. Moreover, the LRS does not seem to be stable without an external bias. It returns to the original higher-resistance state (HRS) with a decrease in bias, as indicated by sweeping the bias near 0 V. Typically, this switching phenomenon could be attributed to threshold RS switching. A similar phenomenon has been observed in a NiO film by Chang et al. [22]; they proposed that this instability of the lower-resistance state is the main difference between observed memory RS switching and threshold RS. In addition, the V_{set} regions varied with the Ta_2O_5 film thickness. The resistance-switching V_{set} regions of the structured Ta_2O_5 films with 68, 119, and 173 nm thickness occurred from 0.65 V to 0.98 V (Fig. 3a), 1.1 V to 1.28 V (Fig. 2b), and 2.6 V to 2.9 V (Fig. 3c), respectively. These variations in the V_{set} value regions indicate that the thickness of the film may be one of the key parameters that affect the SET voltage of resistance switching.

The resistance-switching mechanism of transition-metal oxides remains in debate, and several models have been proposed [23–25]. For tantalum oxide, suboxides of Ta, such as TaO and TaO_2, have higher conductivity than that of Ta_2O_5. A redox reaction process between Ta_2O_5 and TaO_2 has been mostly suggested to understand the resistance-switching behaviors in Ta_2O_5 films [25]. To present amorphous TaO_x with plenty of oxygen vacancies, similarly, a schematic diagram of the resistance-switching mechanism may be proposed as shown in Fig. 4. A tantalum suboxide film, TaO_x, that acts as a conductor, was placed between the metallic substrate and the outer Ta_2O_5 layer. TaO_x plays a key role in the electric field enhancement, which promotes the aggregation of oxygen vacancies between the insulator layer and the Ta metal, as similar investigations on Pt/TaO_x/Ta_2O_5/Pt devices have shown [26]. The CFs formed by the aggregation of nonstoichiometric TaO_x exhibit a conical shape with a large diameter at the positive-biased electrode [27–29]. In Fig. 4b, the TaO_x conducting layer near the Ta/Ta_2O_5 interface could serve as a series resistance and oxygen sink, which provided the 'broad base' for the CFs. Electrons injected from the cathode were trapped by the Ta^{5+} metal cation according to the cathodic deposition reaction, $Ta^{5+} + ne^- \rightarrow Ta^{(5-n)}$. The trapped electrons indicate the existence of nonstoichiometric TaO_x, a more conductive Ta-rich phase, when a positive voltage was applied to the top electrode. The TaO_x growing directly on the anode forms

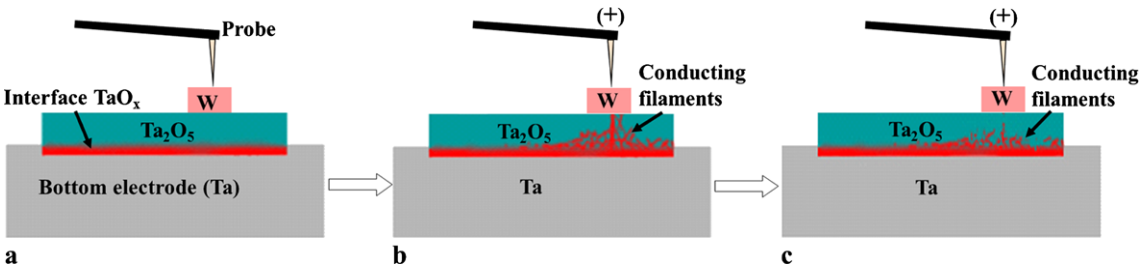

Fig. 4 Schematic diagrams for the proposed unipolar resistance switching of a $W_{TE}/Ta_2O_5/Ta$ structure

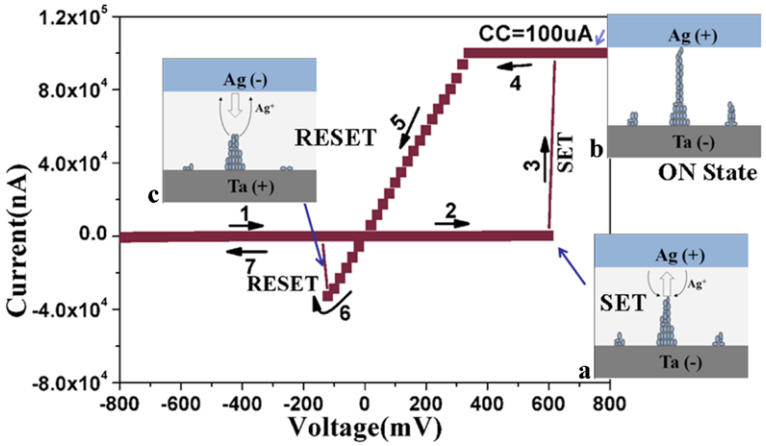

Fig. 5 Typical *I–V curve* of the $Ag_{TE}/a\text{-}Ta_2O_5/Ta$ electrochemical metallization cell, which was switched on by applying a positive bias and switched off by applying a negative bias. *Insets* (**a**), (**b**), and (**c**) are the proposed different states of the switching processes

cone-shaped CFs that electrically connect the top and bottom electrodes. The resulting SET operation switched the device into the LRS. The naturally formed TaO_x conducting layer at the interfaces may be responsible for the smaller SET voltages [30].

The abrupt increase in resistance at the RESET transition may be attributed to the dissolution of some parts of the CFs due to Joule heating from the high current (Fig. 4c) while the voltage is sweeping from V_{max} to zero in the positive-bias region. In addition, the only thermodynamically stable phases in the Ta–O system are metallic Ta (O) solid solution and an insulating Ta_2O_5. The unstable threshold switching, on the other hand, indicates that the metastable TaO_x phase may form and evolve during the switching operation and Joule heating process. A steady and uniform decrease in the diameters of the conductive filaments may have occurred, resulting in the obvious increase in V_{set} with the increase in the Ta_2O_5 layer thickness during the SET process. In addition, the $W_{TE}/a\text{-}Ta_2O_5/Ta$ system cannot be switched from the HRS to the LRS while a negative voltage is applied to the top electrode. Under this bias polarity, the nonstoichiometric phase is easily oxidized into the insulating Ta_2O_5 according to the electric field-controlled movement of the oxygen vacancies, thereby increasing the difficulty in building a continuous, conductive filament between the top and bottom electrodes.

Except for the unipolar threshold RS in a TaO_x-based device with W as the top electrode, Ag metal with the same geometry as the top electrode was also investigated. Distinctly, the typical *I–V* characteristics of the $Ag_{TE}/a\text{-}Ta_2O_5/Ta$ devices show bias polarity dependent resistance switching (Fig. 5) with an obvious bipolar switching characteristic. Different forming processes can be achieved in the $Ag_{TE}/a\text{-}Ta_2O_5/Ta$ and $W_{TE}/a\text{-}Ta_2O_5/Ta$ devices by applying a positive voltage bias prior to performing resistance switching. Therefore, the CF material of the $Ag_{TE}/a\text{-}Ta_2O_5/Ta$ structures may be greatly different from that of the $W_{TE}/a\text{-}Ta_2O_5/Ta$ structures, because the CFs are created during a forming process [31] that is dependent on the top electrode.

Figure 6a shows that the *I–V* characteristic of the $Ag_{TE}/a\text{-}Ta_2O_5/Ta$ system at HRS in a double-logarithmic scale is linear (ohmic) in the low-voltage regime. However, the current begins to increase nonlinearly in the higher-voltage regime. The nonlinear region plotted in a log versus log scale can be fitted further to create a linear curve in a $\ln(I/V)$ versus square-root of voltage plot (Fig. 6b), which coincides with the Poole–Frenkel behavior [32, 33]. A sharp current increase can be obtained at V_{set}, and the system then switches to the LRS. This stage also can be explained by the formation of CFs, similar to the SET process of the $W_{TE}/a\text{-}Ta_2O_5/Ta$ system. However, the CFs extend from the Ag electrode to the bottom Ta electrode as a result

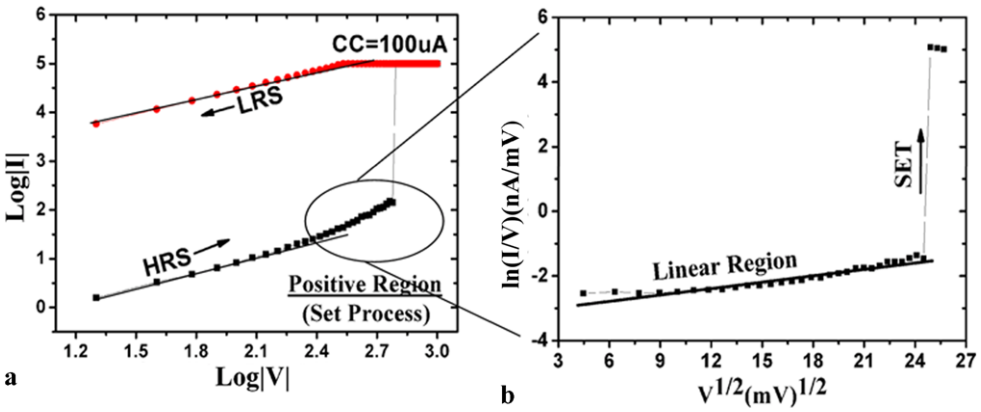

Fig. 6 (**a**) Double-logarithmic plots of the *I–V curve* in the positive-bias region. (**b**) The Poole–Frenkel plot of a high-resistance-state (HRS) $Ag/a\text{-}Ta_2O_5/Ta$ structure at room temperature

of electrochemically active metal deposition and dissolution [34, 35]. The insets (a), (b), and (c) in Fig. 5 schematically show the possible behaviors of CFs during an *I–V* switching cycle. In the initial HRS (a), the active metal (Ag) on the inert electrode shows no electrodeposition. The oxidation of Ag atoms to Ag^+ ions in the Ag anode ($Ag \rightarrow Ag^+ + e^-$) occurred when a positive bias voltage was applied to the top electrode. The Ag^+ cation then migrated through the Ta_2O_5 thin film under a high electric field. Electrochemical reduction and electrocrystallization of Ag on the surface of the cathode ($Ag^+ + e^- \rightarrow Ag$) occurred (a). The randomness of the CF growth process is likely due to the stochastic characteristics of the nucleation behaviors [36]. After the Ag filament had sufficiently grown to create a galvanic metallic contact to the opposite Ag electrode, the device switched to the ON state (b). The electrochemical dissolution of the Ag filament occurred when a sufficiently high negative bias voltage was applied to the top electrode and the RESET stage (c) was achieved.

Based on the electrode effect results, the use of W and Ag as electrode materials of the oxide films may trigger a completely different switching mode to come into play. The Ag electrode, as an active metal, can be more easily oxidized than W when it comes into contact with the surface of a Ta_2O_5 film and is electrodeposited inside the Ta_2O_5 thin film as CFs. This behavior is similar to the proposed formation and rupture behavior of CFs based on cation migration and electrochemical redox reactions [37].

4 Conclusion

In summary, we presented the facile fabrication of a-Ta_2O_5 thin films with tunable thickness through the anodic electrochemical oxidation of Ta-metal foils. The sandwich structures of $W_{TE}/a\text{-}Ta_2O_5/Ta$ and $Ag_{TE}/a\text{-}Ta_2O_5/Ta$ systems with different top electrode materials were intentionally made for investigating the electrode-related resistance-switching phenomenon. We observed the unipolar threshold switching behavior in a $W_{TE}/a\text{-}Ta_2O_5/Ta$ device, while bipolar switching was demonstrated in an $Ag_{TE}/a\text{-}Ta_2O_5/Ta$ device. Both switching mechanisms could be understood by considering the electrochemical formation and rupture of conducting channels inside amorphous Ta_2O_5 films. With W metal as top electrode, the unipolar threshold switching could result from the formation and rupture of nonstoichiometric Ta-rich oxide phases, while with active Ag as top electrode, the growth and dissolution of Ag metal bridges may be responsible for the bipolar switching operation. The thickness of the amorphous Ta_2O_5 film shows an obvious effects on the SET voltage in a $W_{TE}/a\text{-}Ta_2O_5/Ta$ device, but no great effect in an $Ag_{TE}/a\text{-}Ta_2O_5/Ta$ device.

Acknowledgements This work was supported in part by the National Natural Science Foundation of China (Grant Nos. 10974204 and 50931002) and the Hundred Talent Program of the Chinese Academy of Sciences.

References

1. R. Waser, M. Aono, Nat. Mater. **6**, 833 (2007)
2. D.P. Oxley, Electrocomp. Sci. Technol. **3**, 217 (1977)
3. I. Hwang, M.J. Lee, G.H. Buh, J. Bae, J. Choi, J. Kim, S. Hong, Y. Kim, I. Byun, S. Lee, S. Ahn, B. Kang, S. Kang, B. Park, Appl. Phys. Lett. **97**, 052106 (2010)
4. Y.H. Do, J.S. Kwak, J.P. Hong, K.H. Jung, H.S. Kim, J. Appl. Phys. **104**, 114512 (2008)
5. Z.Q. Wang, X.H. Li, H.Y. Xu, W. Wang, H. Yu, X.T. Zhang, Y.X. Liu, Y.C. Liu, J. Phys. D, Appl. Phys. **43**, 385105 (2010)
6. C.H. Cheng, P.C. Chen, S.L. Liu, T.L. Wu, H.H. Hsu, A. Chin, F.S. Yeh, Solid-State Electron. **62**, 90 (2011)
7. V.Sh. Yalishev, Y.S. Kim, B.H. Park, Sh.U. Yuldashev, Appl. Phys. Lett. **99**, 012101 (2011)
8. T. Menke, R. Dittmann, P. Meuffels, K. Szot, R. Waser, J. Appl. Phys. **106**, 114507 (2009)
9. C.H. Liang, K. Terabe, T. Hasegawa, M. Aono, Appl. Phys. Express **1**, 064002 (2008)
10. W.G. Kim, S.W. Rhee, Microelectron. Eng. **87**, 98 (2010)
11. D.S. Jeong, H. Schroeder, R. Waser, Electrochem. Solid-State Lett. **10**, 51 (2007)
12. L. Goux, J.G. Lisoni, M. Jurczak, D.J. Wouters, L. Courtade, Ch. Muller, J. Appl. Phys. **107**, 024512 (2010)

13. C.Y. Lin, C.Y. Wu, C.Y. Wu, T.C. Lee, F.L. Yang, C. Hu, IEEE Electron Device Lett. **28**, 366 (2007)
14. C.Y. Lin, C.Y. Wu, C.Y. Wu, T.Y. Tseng, C. Hu, J. Appl. Phys. **102**(094), 1011 (2007)
15. C.Y. Lin, C.Y. Wu, C.Y. Wu, C.C. Lin, T.Y. Tseng, Thin Solid Films **516**, 444 (2007)
16. T. Tsuruoka, K. Terabe, T. Hasegawa, M. Aono, Nanotechnology **21**, 425205 (2010)
17. C.J. Yang, C. Chen, P.W. Wu, J. Mater. Res. **22**, 4 (2007)
18. L.J. Zhang, R. Huang, M.H. Zhu, S.Q. Qin, Y.B. Kuang, IEEE Electron Device Lett. **31**, 9 (2010)
19. Y. Tsuji, T. Sakamoto, N. Banno, H. Hada, M. Aono, Appl. Phys. Lett. **96**, 023504 (2010)
20. H. El-Sayed, S. Singh, M.T. Greiner, P. Kruse, Nano Lett. **6**, 2995 (2006)
21. C.C. Sheng, Y.Y. Cai, E.M. Dai, C.H. Liang, Chin. Phys. B **21**, 088101 (2012)
22. S.H. Chang, J.S. Lee, S.C. Chae, S.B. Lee, C. Liu, B. Kahng, D.W. Kim, T.W. Noh, Phys. Rev. Lett. **102**, 026801 (2009)
23. K. Shibuya, R. Dittmann, S. Mi, R. Waser, Adv. Mater. **22**, 411 (2010)
24. T. Sakamoto, K. Lister, N. Banno, Appl. Phys. Lett. **91**, 092110 (2007)
25. Z. Wei, Y. Kanzawa, K. Arita, Y. Katoh, K. Kawai, S. Muraoka, S. Mitani, S. Fujii, K. Katayama, M. Iijima, T. Mikawa, T. Ninomiya, R. Miyanaga, Y. Kawashima, K. Tsuji, A. Himeno, T. Okada, R. Azuma, K. Shimakawa, H. Sugaya, T. Takagi, R. Yasuhara, K. Horiba, H. Kumigashira, M. Oshima, IEDM Tech Dig. 293 (2008)
26. H. Yoo, S. Lee, J. Lee, S. Chang, M. Yoon, Y. Kim, B. Kang, M. Lee, C. Kim, B. Kahng, T. Noh, Appl. Phys. Lett. **98**, 183507 (2011)
27. D. Kwon, K. Kim, J. Jang, J. Jeon, M. Lee, G. Kim, X. Li, G. Park, B. Lee, S. Han, M. Kim, C. Hwang, Nat. Nanotechnol. **5**, 148 (2010)
28. K.M. Kim, C.S. Hwang, Appl. Phys. Lett. **94**, 122109 (2009)
29. J. Lee, E. Bourim, W. Lee, J. Park, M. Jo, S. Jung, J. Shin, H. Hwang, Appl. Phys. Lett. **97**, 172105 (2010)
30. T. Hasegawa, K. Terabe, M. Aono, Appl. Phys. Lett. **91**, 092110 (2007)
31. K. Kinoshita, T. Tamura, M. Aoki, Y. Sugiyama, H. Tanaka, Appl. Phys. Lett. **89**, 103509 (2006)
32. T. Babeva, E. Atanassova, Phys. Status Solidi **202**, 330 (2005)
33. J. Frenkel, Phys. Rev. **54**, 647 (1938)
34. C. Schindler, G. Staikov, R. Waser, Appl. Phys. Lett. **94**, 072109 (2009)
35. Q. Liu, S.B. Long, H.B. Lv, W. Wang, J.B. Niu, Z.L. Huo, J.N. Chen, M. Liu, ACS Nano **4**, 6162 (2010)
36. R. Waser, R. Dittmann, G. Staikov, K. Szot, Adv. Mater. **21**, 2632 (2009)
37. C.C. Lin, B.C. Tu, C.C. Lin, C.H. Lin, T.Y. Tseng, IEEE Electron Device Lett. **27**, 725 (2006)